Desalination and Water Treatment
www.deswater.com
doi: 10.5004/dwt.2023.29290

285 (2023) 167–179
February

Adsorption of Cu(II) and Cd(II) with graphene based adsorbent: adsorption kinetics, isotherm and thermodynamic studies

Sobur Ahmed[a,b], Fatema-Tuj-Zohra[a,b], Tasrina Rabia Choudhury[c], Md. Zahangir Alam[b], Mohammad Nurnabi[b,*]

[a]*Institute of Leather Engineering and Technology, University of Dhaka, 44-50, Hazaribagh, Dhaka-1209, Bangladesh, emails: soburahmed@du.ac.bd (S. Ahmed), fatema.ilet@du.ac.bd (F.-T. Zohra)*
[b]*Department of Applied Chemistry and Chemical Engineering, University of Dhaka, Dhaka-1000, Bangladesh, Tel.: +8801552428255; Fax: +880-2-9667222; emails: nnabi@du.ac.bd (M. Nurnabi) ORCID: http://orcid.org/0000-0001-8245-6535, zahangir@du.ac.bd (Md. Z. Alam)*
[c]*Analytical Chemistry Lab, Atomic Energy Center, Bangladesh Atomic Energy Commission, Dhaka, Bangladesh, email: tasrina.rabia@gmail.com (T.R. Choudhury)*

Received 26 July 2022; Accepted 1 January 2023

ABSTRACT

In this study, graphene oxide (GO) adsorbent was prepared from commercial graphite powder and characterized using a variety of analytical methods, including X-ray diffraction, X-ray photoelectron spectroscopy, field-emission scanning electron microscopy, Fourier-transform infrared spectroscopy, zeta potential, dynamic light scattering and Brunauer–Emmett–Teller analysis. Batch experiments were conducted to investigate the effect of pH, adsorbent dosage, contact time and metal ions concentrations for adsorptive removal of Cu(II) and Cd(II) ions from aqueous solutions. The kinetics, adsorption isotherms, and thermodynamics were studied to determine the adsorption mechanism. The results showed that at pH higher than 3.5 (pH_{zpc}), carboxyl group of GO was deprotonated to make the surface negatively charged, which was advantageous for metal ions adsorption. It was also evident that the optimum pH for removal of Cu(II) was 5.0, while that of Cd(II) was 7.0. The adsorption processes of Cu(II) and Cd(II) followed both the Langmuir and Freundlich isotherms, indicating complex nature of the adsorption processes. The maximum adsorption capacities (q_{max}) of GO for Cu(II) and Cd(II) calculated from Langmuir isotherms were 193.05 and 231.45 mg/g, respectively. The kinetics studies showed that adsorption processes for both the metal ions followed pseudo-second-order reaction model. Thermodynamic investigations revealed the adsorption process as exothermic and spontaneous at room temperature. Regeneration and reuse of spent adsorbents were also studied and found that regenerated GO demonstrated lower adsorption capacities compared to the fresh GO.

Keywords: Environmental conservation; Graphene oxide; Heavy metals; Ionization; Water treatment; Zeta potential

1. Introduction

Availability and supply of safe water is of great interest for human and other living organisms since the quality of water straight way impacts on them. As a result of fast urbanization and industrialization, sources of water are getting polluted everyday with metals, such as chromium, cadmium, copper, lead, mercury, and the polluted water causes severe crisis to the biological systems [1,2]. The disposal rate of synthetic chemicals and waste into water

* Corresponding author.

environment is increasing day by day and worsening the situation alarmingly [3]. Common heavy metal contaminants are non-biodegradable, toxic, persistent in nature and have the tendency of accumulation, which lead to ecological imbalances and pose severe risk to human and the environment [4–8]. Currently, remediation of water pollution caused by heavy metals has drawn much attention of the scientific community [9,10].

Several techniques, such as precipitation, membrane filtration, electroplating, ion exchange, and adsorption are some of the traditional processes for heavy metal decontamination [11,12]. However, few significant demerits of these methods such as requirements of high amount of chemicals and energy, formation of hazardous sludge, high cost at large scale and low efficiency at metal concentrations below 100 mg/L [13–15] restricted their wide application. As a relatively simple process, adsorption method is widely used in heavy metals removal and considered renewable and of low energy consumption [16,17]. Some common adsorbents are activated carbon [18,19], clay minerals [20], natural zeolites [21], chitosan [22] and alginates [23]. Adsorption is preferred because of high removal efficiency, low cost and generation of less amount of secondary pollutant/sludge [24]. However, the mostly used adsorbents, for example, activated carbon are of high cost, selective, and difficult to produce in large scale [25]. Agricultural and household biomass-based materials are available, chief and showed noticeable adsorption capacity for metals and metal ions [26]. However, most of those adsorbents are inefficient and have low adsorption capacity.

Nanomaterials retain an enormous surface area, stable surface charge and chemical configuration, which make them attractive for various applications including heavy metals removal [27]. In comparison to other nano adsorbent materials, graphene oxide (GO) contains functional groups such as hydroxyl, epoxy, carboxylic groups [28–30], and possesses high surface area (2,630 m^2/g), good machinability, chemical inertness and hydrophilicity [31–34]. These oxygen containing functional groups poses excellent adsorption capacity for wide range of contaminants [35–37] and thus GO and its composites have drawn much attention in water filtration research [38]. In comparison to pristine graphene, the active functional groups and the base graphene material produce a highly effective adsorbent with superior structural and functional properties [39]. The objectives of this work was to synthesize and apply graphene oxide for adsorption of Cu(II) and Cd(II) from aqueous solutions. The research explored the effectiveness of prepared graphene oxide for removal of copper(II) and cadmium(II) ions with insight studies on the equilibrium, kinetics and thermodynamics of the adsorption processes.

2. Materials and methods

2.1. Materials

Copper chloride ($CuCl_2{\cdot}2H_2O$) and cadmium sulfate ($3CdSO_4{\cdot}8H_2O$) were used to prepare the standard solution of copper(II) and cadmium(II). GO was prepared by oxidizing graphite powder (99.5%) with H_2SO_4 (98%), HNO_3 (65%), $KMnO_4$ (97%), $NaNO_3$, H_2O_2 (30%) and HCl (37%). The chemicals were purchased from different sources, such as H_2SO_4 and HNO_3 from Active Fine Chemicals (Bangladesh), $NaNO_3$ from Unichem (China), graphite powder, $KMnO_4$ and H_2O_2 from Merck (India), HCl from RCI Labscan (Thailand), copper chloride and cadmium sulfate from Qualikems (India). All chemicals were of analytical grade and used as received.

2.2. Graphene oxide preparation

GO was prepared by following modified Hummer's method as mentioned in our previous work [40]. Briefly, a mixture of concentrated H_2SO_4 and HNO_3 (3:1 ratio, 75 mL) was taken in a round bottom flask, cooled in an ice bath and followed by addition of graphite powder (3.0 g), $KMnO_4$ (9 g) and $NaNO_3$ (1.5 g) over a period of 2 h under vigorous stirring and left overnight at room temperature to form a thick paste. The mixture was then diluted with deionized (DI) water (120 mL) and agitated at 35°C for 4 h in an oil bath to afford a deep brown mixture. Again, DI water (420 mL), 30% H_2O_2 (20 mL) and 5% HCl (200 mL) were added to the mixture under stirring to obtain GO as a suspension. The suspension was washed several times by adding DI water followed by centrifugation until neutralization.

2.3. Characterization methods

Prepared GO was characterized by different instrumental techniques. The functional groups were identified with Fourier-transform infrared spectroscopy (FT-IR; Prestige-21, Shimadzu, Japan). The morphology, surface structure and chemical nature and crystalline properties of GO were studied with X-ray photoelectron spectroscopy (XPS; K-ALPHA, Thermo Fisher Scientific, Czech Republic), field-emission scanning electron microscopy (FE-SEM; JSM-7610F, JEOL) and X-ray diffraction (Ultima IV, Cu Kα radiation, 40 kV, 1.64 mA, λ = 0.154 nm, 5°–100°), respectively. The surface charge and ionic nature of GO was measured with a zeta potential analyzer, Malvern Zetasizer (Nano-ZS ZEN 3600). The Brunauer–Emmett–Teller (BET) surface area, pore volume and pore size distribution of GO was analyzed with BET sorptometer (Model no. BET-201-A, PMI, USA) and particle size was measured with particle size analyser (Model: Litesizer 500, Anton Paar) through dynamic light scattering (DLS) method.

2.4. Parameter exploration and data treatment

The adsorption of Cu(II) and Cd(II) on GO was studied using batch equilibrium adsorption method [41]. To investigate the effects of related factors for adsorption process, that is, pH, dosage of adsorbent, initial concentration of Cu(II) and Cd(II) and contact time, a number of experiments were conducted. Atomic absorption spectroscopy (AAS) was used to determine the metal ion concentrations. The adsorption at time t, q_t (mg/g) and percentage removal was calculated by Eqs. (1) and (2), respectively. Adsorption at equilibrium, q_e (mg/g) was found employing Eq. (3):

$$\text{Adsorption capacity at time } t,\ q_t = \frac{\left(C_0 - C_t\right)V}{W} \tag{1}$$

$$\%\ \text{of removal}\ \%\ \text{of removal} = \frac{\left(C_0 - C_e\right)}{C_0} \times 100 \quad (2)$$

$$\text{Adsorption capacity at equilibrium, } q_e = \frac{\left(C_0 - C_e\right)V}{W} \quad (3)$$

where C_o is initial concentration of metal ion (mg/L), C_t is concentration of metal ion at time t (mg/L), C_e is concentration of metal ion at equilibrium (mg/L), V is volume of the metal ion solution (L), and W is mass of the adsorbent (g).

The equilibrium of adsorption process was explained using the Langmuir [Eq. (4)] and Freundlich [Eq. (6)] isotherms.

$$\frac{C_e}{q_e} = \frac{1}{q_m b} + \frac{1}{q_m} C_e \quad (4)$$

$$R_L = \frac{1}{1 + C_m b} \quad (5)$$

$$\ln q_e = \ln K_F + \frac{1}{n} \ln C_e \quad (6)$$

where C_e is equilibrium metal ion concentration (mg/L), b is Langmuir constant (L/mg), q_e and q_m are equilibrium adsorption (mg/g) and theoretical maximum adsorption capacity (mg/g), respectively. According to the Langmuir model, the theoretical maximum adsorption capacity q_m was calculated by plotting the value of C_e/q_e vs. C_e. To determine the favorable nature of adsorption process, the separation factor R_L value was calculated using Eq. (5) where R_L is separation factor, C_m is the maximum initial metal ion concentration employed in the experiments.

To investigate the kinetics of the adsorption process, pseudo-first-order model and pseudo-second-order models were evaluated according to Eqs. (7) and (8), respectively.

$$\log\left(q_e - q_t\right) = \log q_e - \left(\frac{k_1}{2.303}\right) t \quad (7)$$

$$\frac{t}{q_t} = \left(\frac{1}{k_2 q_e^2}\right) + \left(\frac{1}{q_e}\right) t \quad (8)$$

where, k_1, k_2 are the rate constants (g/mg·min), q_e is adsorption at equilibrium (mg/g), q_t is adsorption at time t (mg/g).

For thermodynamic analysis, the Gibb's free energy change (ΔG) was calculated according to Eqs. (9) and (10).

$$\Delta G = -RT \ln k_d \quad (9)$$

where R is the universal gas constant (8.314 J/mol·K), k_d is the distribution coefficient for the equilibrium sorption and T is the absolute temperature (K).

$$k_d = \frac{q_e}{C_e} \quad (10)$$

The linearized van't Hoff isotherm Eq. (11) was used to determine the change of enthalpy (ΔH) and entropy (ΔS).

$$\ln k_d = \frac{-\Delta H}{RT} + \frac{\Delta S}{R} \quad (11)$$

3. Results and discussion

3.1. Characterization

3.1.1. XPS analysis

The XPS spectra of GO (Fig. 1a) showed the strong signals for C and O with corresponding binding energy [42]. The peaks at 284.82, 286.82, 288.28, and 290.90 eV were assignable to C–C/C–H, C–O, C=O, and O–C=O types of carbon, respectively (Fig. 1b), while the peaks at 532.74 and 531.43 eV were assignable to C=O and C–O types of oxygen, respectively (Fig. 1c). Similar XPS spectrum of GO were observed in previous studies [43].

3.1.2. Microscopic analysis

Morphological characterization of GO before and after adsorption of copper and cadmium ions were studied using FE-SEM and represented in Fig. 2. The images were captured at 10,000X magnification and 6.6–7.6 mm working distance with 5.0 kV. A randomly wrinkled fluffy sheets were observed that contribute the major roles in metal adsorption [44]. Similar result was documented by a previous study of metal ions adsorption by GO [45].

The image of copper and cadmium ions loaded GO showed a slightly different surface as evident in Fig. 2b and c. A similar effect had been documented for adsorption of Cu(II) onto GO and GO nanoparticles [46].

3.1.3. Spectral analysis

FT-IR spectra of GO, Cu(II) and Cd(II) loaded GO are shown in Fig. 3 with some distinct adsorption peaks at different wave numbers in the infrared region indicating the presence of diverse functional groups. Strong and broad O–H stretching vibration band at 3,583 cm^{-1}, C–H stretching vibration at 3,182 cm^{-1}, C=O stretching vibration band of the carboxylic group at 1,689 cm^{-1}, aromatic C=C stretching band at 1,535 cm^{-1}, symmetric C–O stretching in the C–O–C group at 1,400 cm^{-1}, and the epoxy C–O band at 999 cm^{-1} were observed. The FT-IR spectra of GO was in agreement to the findings of other investigations [47,48]. The O–H stretching vibration band at 3,583 cm^{-1} was shifted to 3,414 and 3,417 cm^{-1}, while C–H stretching vibration at 3,182 cm^{-1} was shifted to 2,981 and 2,931 cm^{-1} due to adsorption of copper and cadmium ions, respectively.

3.1.4. BET analysis

Surface area, pore volume and pore size/diameter of GO were analyzed through nitrogen sorption system and shown in Fig. 4. The BET analysis recommends that GO has a specific surface area of 127.32 m^2/g which was much lower than the theoretical specific surface area for completely exfoliated and isolated graphene sheets (~2,620 m^2/g)

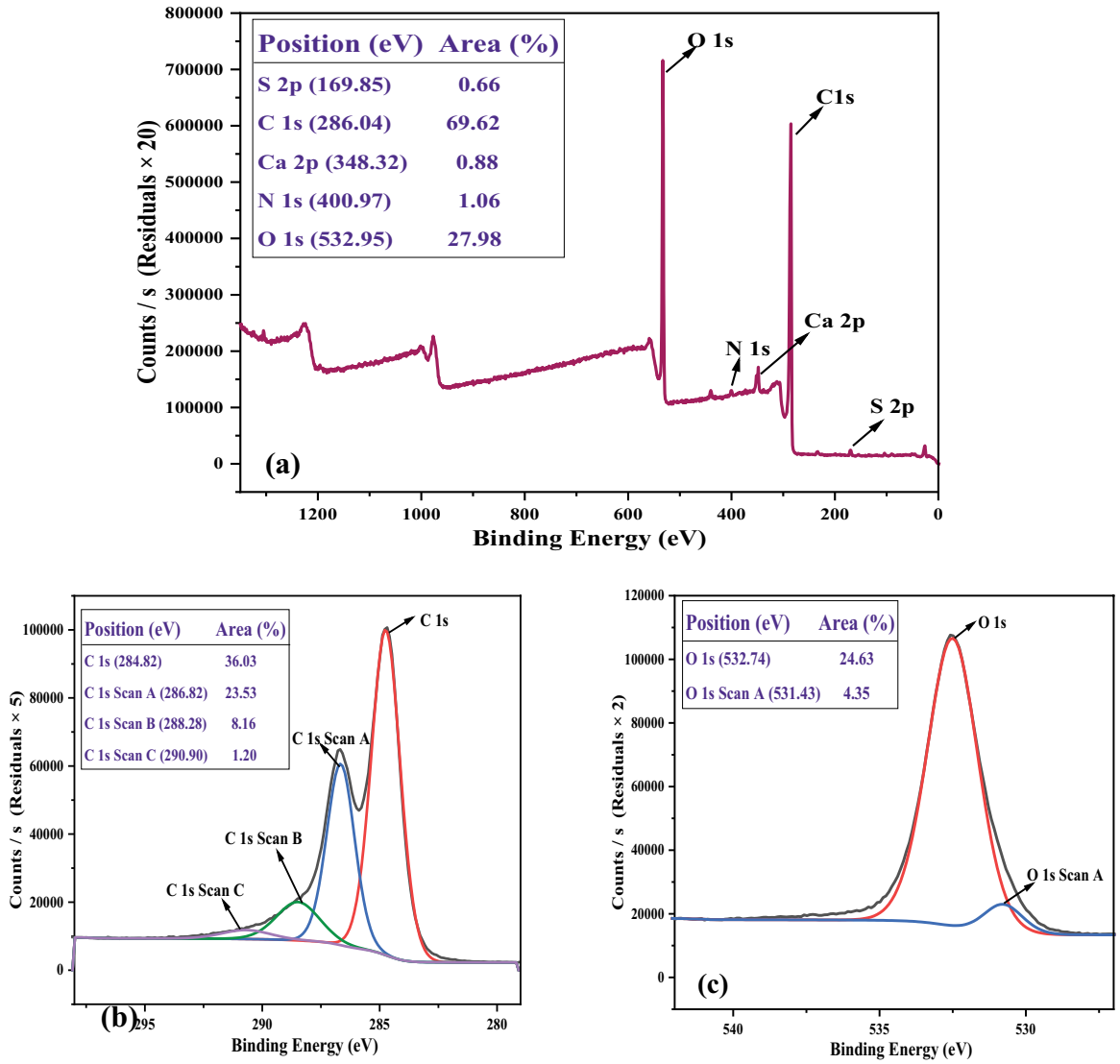

Fig. 1. (a) XPS spectra of GO, (b) types of carbon in GO, and (c) types of oxygen in GO.

[49], which could be due to the agglomeration and overlapping of the GO sheets [50,51]. Barrett–Joyner–Halenda (BJH) method was followed and the average pore size/diameter was found to be 27.47 Å and has a total pore volume of 0.0875 cc/g. These characteristics of GO showed the affinity towards Cu and Cd metal ions.

3.1.5. Particle size analysis

The size of GO particles in DI water was measured by dynamic light scattering (DLS) using Particle Size Analyzer. The particle size of the prepared GO was found to be 665.3 nm (Table 1), which showed good agreement with previous report [52].

3.2. Influence of process factors on adsorption

The efficacy of adsorbent for heavy metal removal depends on various parameters such as pH of the solution, adsorbent dosages, contact time and initial metal concentration, temperature etc. and are discussed in this section.

3.2.1. Effect of pH

pH is an important parameter as it influences the property of adsorbent surface and the nature of the adsorbate [41]. In order to explore the effect of pH on adsorption process, copper(II) solution (166.5 ppm, 20 mL) was taken in each of five conical flasks and the pH was adjusted to 3.0, 4.0, 5.0, 6.0 and 7.0. Then GO (0.039 g) was added to each solution and agitated at 150 rpm for 2 h at room temperature in an orbital shaker. The highest removal percentage of Cu(II) by adsorption was achieved as 76.36% at pH 6.0 and it was observed that copper(II) precipitated at pH > 6.0 (Fig. 5d), thus, pH 6.0 was selected for rest of the adsorption study in case of Cu(II). Similarly, another set of experiments were carried out with cadmium(II) solutions (201.5 ppm, 20 mL) at different pH and observed that precipitation of Cd(II) was

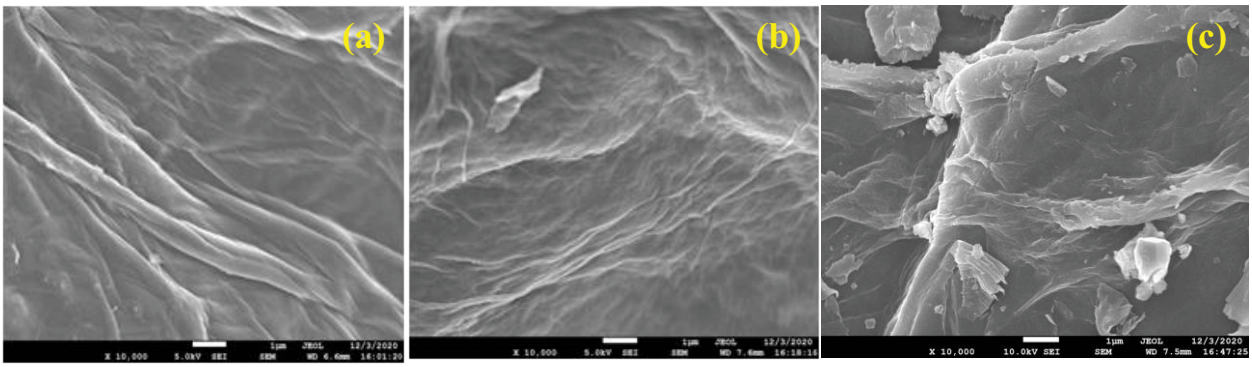

Fig. 2. FE-SEM images of (a) fresh GO, (b) after Cu(II) adsorption, and (c) after Cd(II) adsorption.

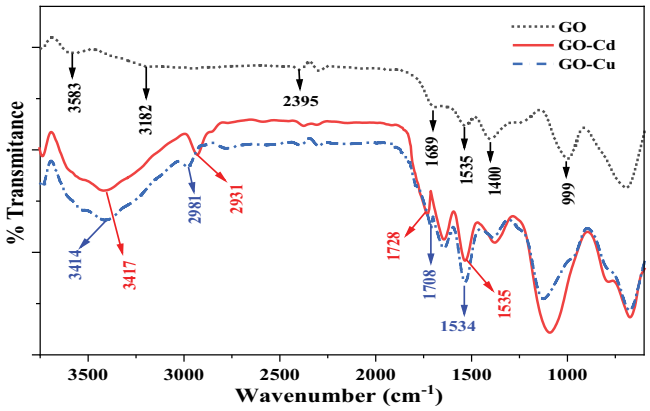

Fig. 3. FT-IR spectra of GO (top), Cu(II) adsorbed GO (bottom) and Cd(II) adsorbed GO (middle).

occurred at pH > 7.0. Therefore, the highest removal percentage by adsorption was found as 87.45% at pH 7.0, which was considered as optimum pH (Fig. 5d) for Cd(II) adsorption. Studies on pH revealed that GO surface had zero charge at pH 3.5 (pH_{zpc}) and below this pH adsorbent surface was positively charged due to protonation of carboxylic group, which resulted electrostatic repulsion with metal ions. Moreover, at lower pH there was a high competition between the H^+ and metal ions, where adsorbent surface was mostly occupied by proton because of its smaller size. Both these phenomena led to lower adsorption of metal ions at lower pH [53,54]. On the other hand, at pH above the ZPC, GO surface became negatively charged due to deprotonation of carboxylic group (Fig. 5a) and resulted electrostatic attraction between the GO surface and metal ions [55]. In addition to that at higher pH the proton concentration was reduced leading to less competition of protons with cations and resulted higher adsorption of metal ions [56].

3.2.2. Effect of adsorbent dosage

Different dosages of GO (0.25, 0.5, 1.0, 1.5, 2.0 and 2.5 g/L) were added to six conical flasks containing standard solution of copper salt (166.5 ppm, 10 mL) at the optimum pH (6.0) and shaken in an orbital shaker at 150 rpm for 2 h. Adsorption and percentage of removal were calculated using Eqs. (1) and (2). It was observed that the adsorption of Cu(II) ion decreased, and the percentage of removal increased with the increase of adsorbent dosage (Fig. 6a). However, at a dosage of 1.0 g/L both q_{max} and percentage removal were satisfactory and this amount was selected as optimum dosage for copper(II) adsorption. Similarly, the optimum dosage of GO for cadmium ion removal was 1.5 g/L. In general, with increasing adsorbent dosages the number of active sites and total surface area increased gradually, allowing maximum metal ions to interact with the active sites [57,58] and resulted gradual increment of removal percentage. However, as the adsorbent dosages increased, the sorption capacity decreases since a significant number of active sites remained unreacted [47].

3.2.3. Effect of contact time and initial metal ion concentration

The impact of contact time and initial concentration of Cu(II) on the adsorption were studied with batch experiments (Fig. 7). In the experiment, 10 mL copper(II) solutions of varied concentrations (99.3, 151.23, 203.6, and 240.3 ppm) were used at optimum pH (6.0) and dosage (1.0 g/L) for a certain time (0–120 min). Fig. 7a illustrates that adsorption process reached at equilibrium just after 20 min for Cu(II). Similarly, 10 mL Cd(II) solutions of different concentrations (103.82, 152.15, 201.40 and 250.65 ppm) were treated with 1.5 g/L at optimum pH (7.0) for certain duration (0–120 min). The equilibrium time for cadmium ion adsorption was also 20 min as illustrated in Fig. 7b. Over the time, adsorbate occupied adsorbent's active sites on the surface as long as it had unoccupied active sites, thus the adsorption capacity increased until equilibrium was reached [25].

The metal ion concentration is a vital factor in the adsorption process, explaining the correlation of mass balance and mass transfer within the solution and adsorbent surface [59,60]. Adsorption increased with an increasing initial metal ion concentration due to higher diffusion rate [6,61].

3.3. Studies on equilibrium isotherms

Equilibrium isotherm study focuses on the adsorption mechanism considering equilibrium between adsorbate in solution and on the surface of adsorbent. It also determines the maximum adsorption capacity (q_m) of an adsorbent. The linear form of Langmuir isotherm represents mono-layer

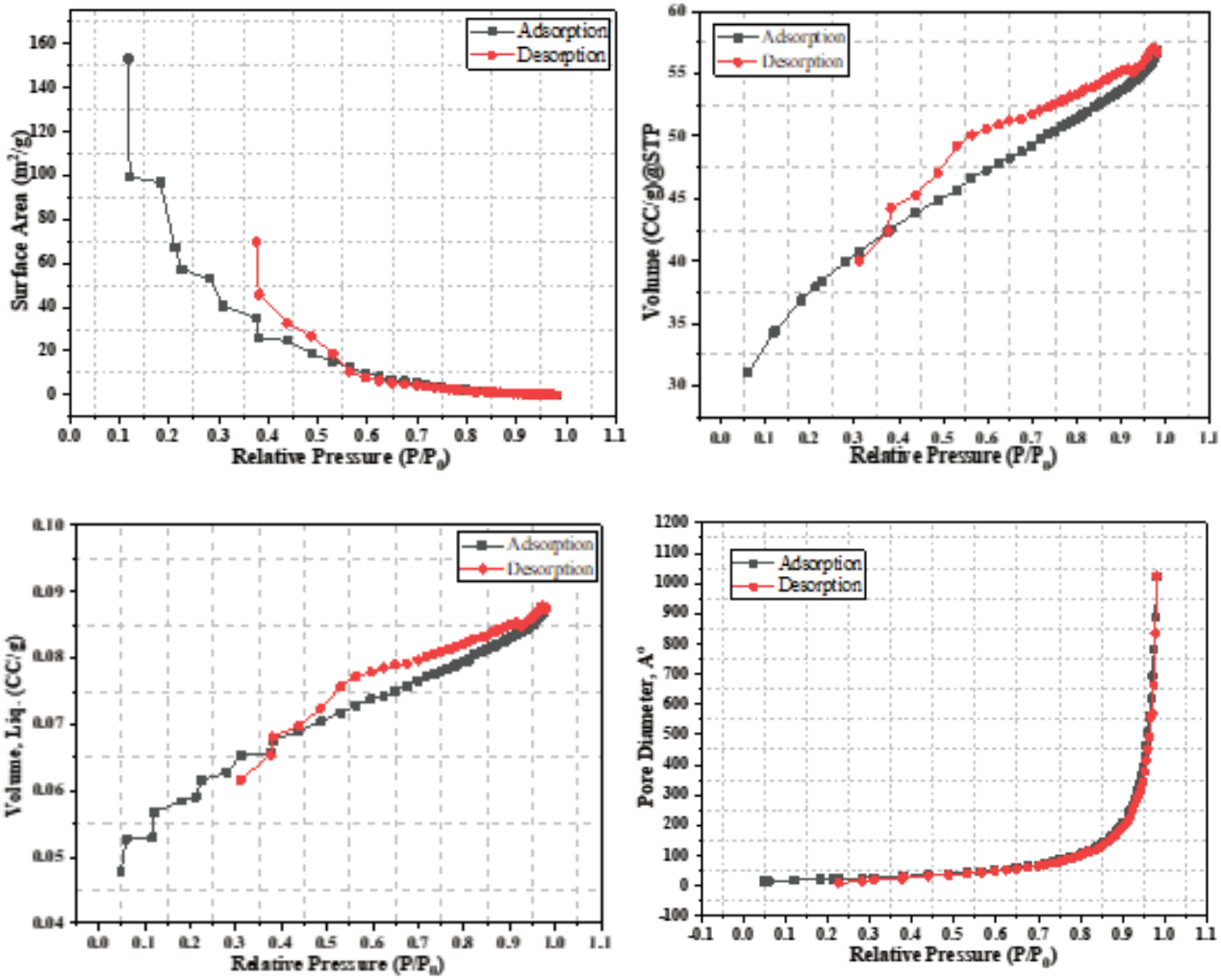

Fig. 4. BET analysis of GO.

Table 1
Particle size of GO

Parameters	Values
Particle size	665.3 nm
Polydispersity index	23.9%
Diffusion coefficient	0.7 μm²/s
Transmittance	75.7%

adsorption process, while Freundlich isotherm indicates non-uniform multilayer distribution of adsorbate molecules.

In the current study the equilibrium adsorption model parameters and the correlation coefficient (R^2) values were calculated using OriginPro 2019B software are listed in Table 2. Considering those parameters and the value of R^2, Cu(II) and Cd(II) adsorption on GO surfaces followed both the Langmuir and Freundlich isotherm models (Fig. S1), which indicated that adsorption of Cu(II) and Cd(II) ions on GO surface complex in nature. The maximum adsorption capacities (q_{max}) were calculated from Langmuir isotherm and found as 193.05 and 231.48 mg/g for Cu(II) and Cd(II), respectively. However, the values of R_L for Cu(II) and Cd(II) were 0.032 and 0.148, respectively, which supported the advantageous monolayer adsorption mechanism [62,63]. The overlapping patterns of several Langmuir-type sorption phenomena occurring at different sites on adsorbents could result Freundlich type isotherms [64]. Therefore, both the Langmuir and Freundlich isotherms were followed at the same time, which was regarded as the composite type isotherm. The composite isotherm was linear since the component Langmuir isotherms were linear.

3.4. Studies on adsorption kinetics

The pseudo-first-order and pseudo-second-order reaction models were utilized to realize the sorption kinetics of Cu(II) and Cd(II) onto GO. Pseudo-first-order model was studied by plotting $\log(q_e - q_t)$ vs. t following Eq. (7) and pseudo-second-order model was studied by plotting t/q_t vs. t according to Eq. (8), where k_2 is the rate constant (g/mg·min).

The results of the experimental data best fitted with pseudo-second-order kinetic model for both the metal ions

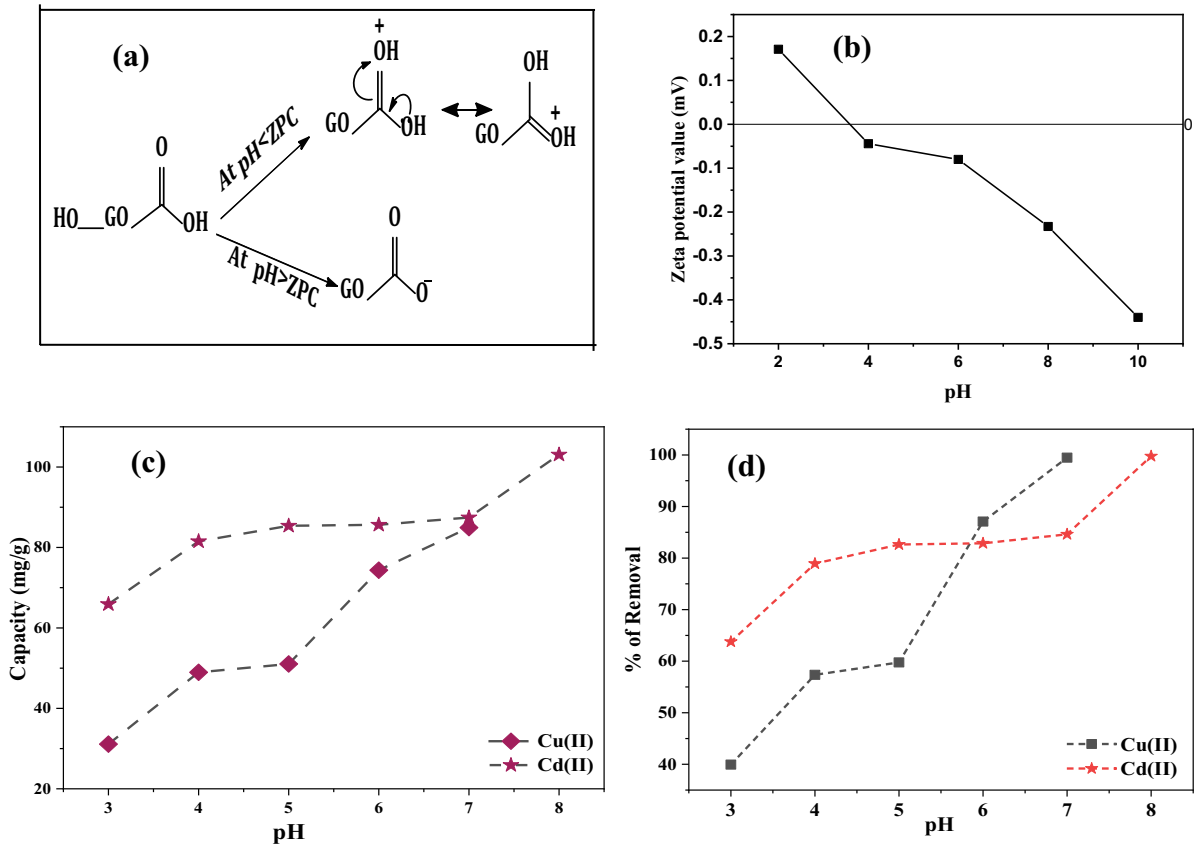

Fig. 5. Effect of pH on (a) ionization of GO, (b) zeta potential value of GO, (c) adsorption capacity of GO for Cu(II) and Cd(II), and (d) % of removal of Cu(II) and Cd(II).

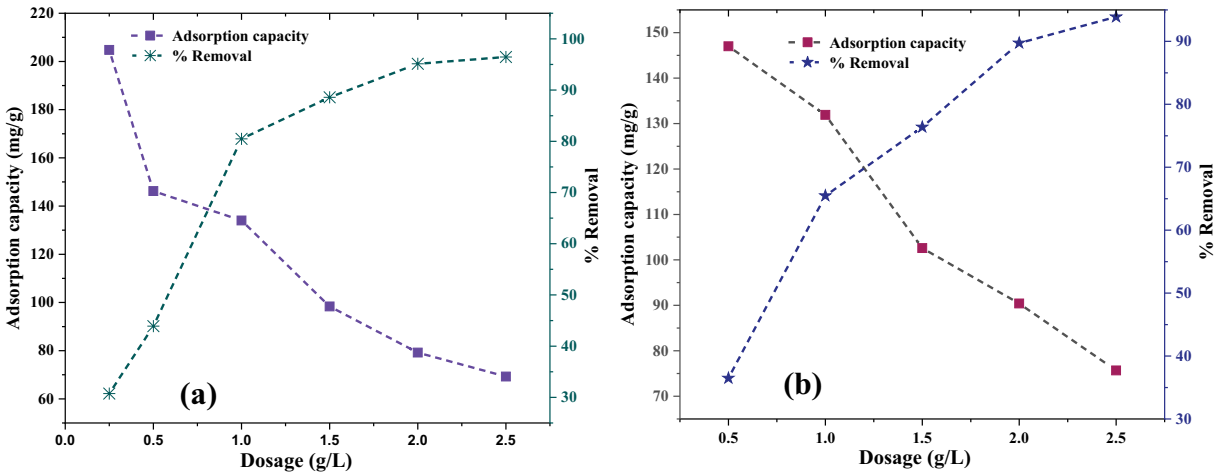

Fig. 6. Effect of adsorbent dosage on (a) Cu(II) adsorption and (b) Cd(II) adsorption on GO.

as the experimental values of q_e matched better with that obtained from pseudo-second-order kinetic model (Table 3, Figs. S2 and S3). The regression coefficient value (R^2) in case of copper (0.998, 0.997, 0.989 and 0.949) and cadmium (0.998, 0.998, 0.999, 0.998) are also supportive of pseudo-second-order model (Tables 3 and 4). Previous studies using GO and derivatives of GO to remove chromium(III) ions from aqueous media yielded comparable results [65,66]. This evidence suggests that the adsorption process is chemisorption type. As a result, a strong attraction force develops between metal ions and the anionic functional groups present in the GO, during the adsorption process, resulting in the

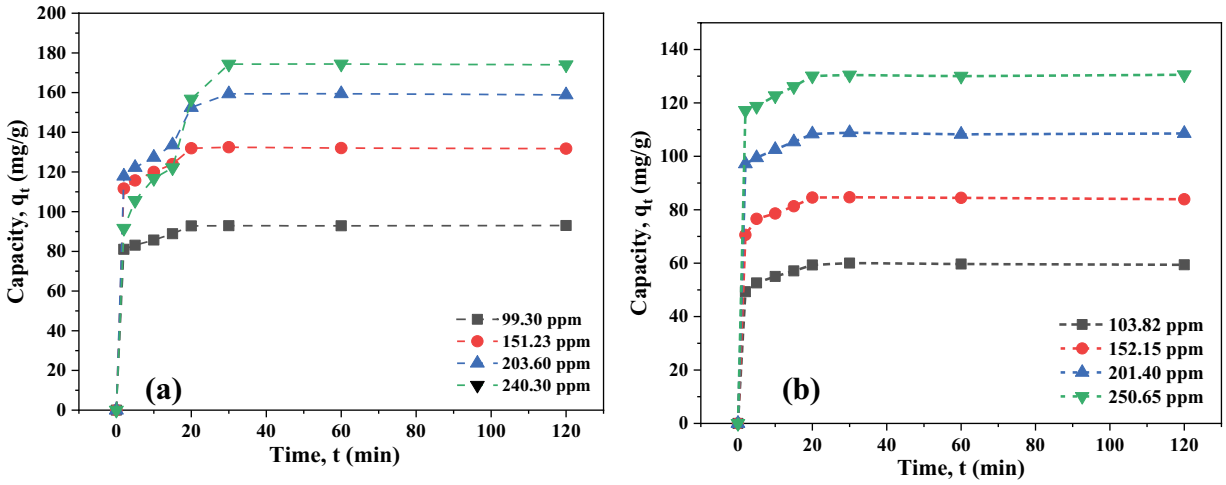

Fig. 7. Effect of initial concentration of (a) Cu(II) and (b) Cd(II) on adsorption on GO over time.

Table 2
Adsorption isotherm constants for Cu(II) and Cd(II) on GO

Langmuir constants	Values Cu(II)	Values Cd(II)	Freundlich constants	Values Cu(II)	Values Cd(II)
q_m (mg/g)	193.05	231.48	k_f	57.230	12.019
b (L/mg)	0.1239	0.0230	n	3.700	1.675
R_L	0.032	0.148	R^2	0.991	0.996
R^2	0.997	0.999			

Table 3
Summary of adsorption kinetics for Cu(II) adsorption on GO

Kinetics model	Parameters	99.3 ppm	151.23 ppm	203.6 ppm	240.3 ppm
Pseudo-first-order	q_e* (mg/g)	92.85	131.97	159.36	174.36
	k_1	0.0817	0.07	0.087	0.074
	R^2	0.973	0.997	0.772	0.802
	q_e** (mg/g)	14.57	23.38	55.98	107.64
Pseudo-second-order	k_2	0.016	0.01	0.0029	0.0012
	R^2	0.998	0.997	0.989	0.949
	q_e** (mg/g)	94.52	133.33	166.1	189.39

*Experimental, **Theoretical

Table 4
Summary of adsorption kinetics for Cd(II) adsorption on GO

Kinetics model	Parameters	103.82 ppm	152.15 ppm	201.4 ppm	250.65 ppm
Pseudo-first-order	q_e* (mg/g)	59.31	84.56	108.37	130.08
	k_1	0.1131	0.1043	0.101	0.092
	R^2	0.993	0.964	0.982	0.971
	q_e** (mg/g)	12.39	15.72	14.47	16.89
Pseudo-second-order	k_2	0.022	0.018	0.0189	0.016
	R^2	0.998	0.998	0.999	0.998
	q_e** (mg/g)	60.68	86.13	109.65	131.41

*Experimental, **Theoretical

formation of electrostatic bonds. Cu and Cd have diagonal relationship in the periodic table, therefore similar adsorption mechanism was expected in the present investigation.

Adsorption through pseudo-second-order indicated that the major uptake mechanisms of Cu(II) and Cd(II) ions might involve ion exchange reaction between metal ions and the protons of various functional groups at adsorption sites of GO. However, involvement of heterogeneous adsorption sites could lead more complex procedure than exchange reactions including weak chemical interactions such as electrostatic interactions and van der Waals forces [39,67].

3.5. Thermodynamics

A thermodynamic evaluation of an adsorption process determines its randomness, spontaneity, and feasibility based on temperature [68]. The thermodynamic parameters such as standard free energy change, enthalpy and entropy change were assessed using van't Hoff equations [69] at different temperatures (293–338 K) (Fig. 8, Table 5).

Considering the free energy change (ΔG) and enthalpy change (ΔH), it was evident that the process was exothermic and spontaneous for both the Cu(II) and Cd(II) adsorption.

3.6. Regeneration and reuse of adsorbent

Regeneration of exhausted/spent adsorbents and their subsequent use is necessary for developing a commercial adsorbent [70,71]. The regeneration experiment was conducted by 2% HCl and reused for Cu(II) and Cd(II) adsorption to investigate the potential for reuse. Regeneration experiments revealed that adsorption capacity gradually declined with recycle of it [72]. Fresh GO had adsorption capacities of 105.61 and 63.13 mg/g for Cu(II) and Cd(II), respectively, whereas adsorption capacities after first, second and third recycle were 91.72, 81.21, and 77.49 mg/g for copper and 61.54, 54.23, and 45.24 mg/g for Cd, respectively (Fig. 9), signifying that regeneration and reuse of GO needs further studies.

3.7. Plausible mechanism of adsorption process

Adsorption occurs when oppositely charged particles come into contact through numerous binding forces such as, electrostatic interactions, hydrogen bonds, dipole–dipole interaction, van der Waals forces and ion-exchange. The two most significant factors to consider during adsorption are surface chemistry and pore volumes. Graphene oxide has a negative surface charge at pH > 3.5 (pH_{ZPC}), which afforded electrostatic interaction with positively charged metal ions. Negative surface charge may be attributed to the dissociation of carboxyl groups of GO. The plausible chelation of metal ions may be represented as Fig. 10.

3.8. Effectiveness of adsorbent

Researchers have focused their attention on GO and its derivatives as promising adsorbents for removing metal ions. A comparison of efficacy of GO synthesized in this study with different adsorbents developed earlier is presented in the Table 6 and found that this study demonstrated much better metals ion adsorption on GO.

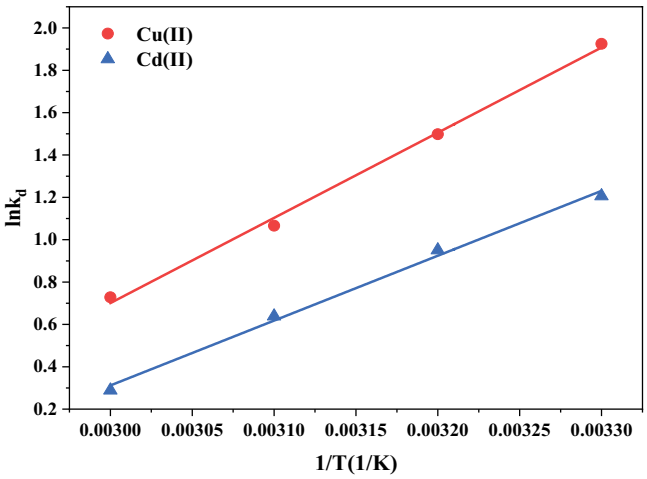

Fig. 8. Plot for van't Hoff isotherm.

Table 5
Thermodynamics parameters for copper(II) and cadmium(II) adsorption

T (K)	ΔG (kJ/mol)		ΔH (kJ/mol)		ΔS (kJ/mol)	
	Cu(II)	Cd(II)	Cu(II)	Cd(II)	Cu(II)	Cd(II)
293	–4.769	–2.987	–33.447	–25.465	–0.0945	–0.0738
308	–3.836	–2.434				
323	–2.818	–1.689				
338	–1.985	–0.788				

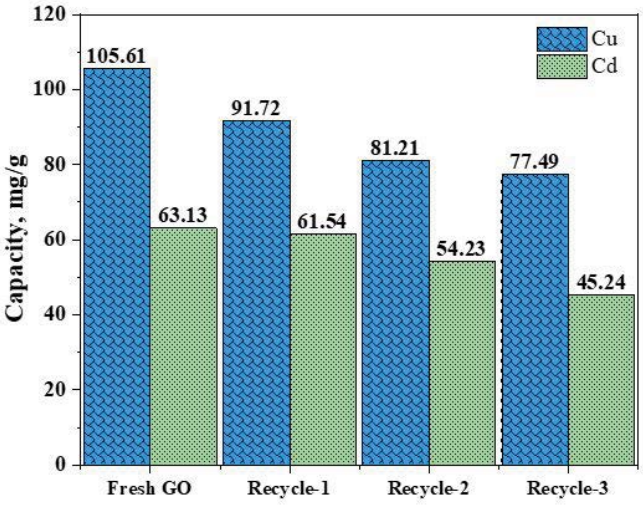

Fig. 9. Adsorbent capacity of regenerated graphene oxide.

4. Conclusions

In this study graphene oxide was synthesized from graphite granules using modified Hummer's method and fully characterized. It was then applied for the removal of two most common heavy metal ions such as Cu(II) and Cd(II). The adsorption process followed both Langmuir and Freundlich isotherms and pseudo-second-order reaction

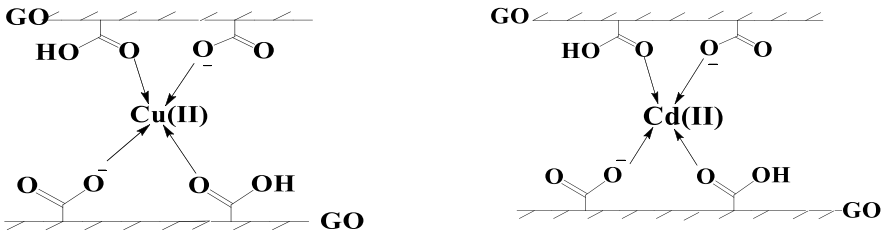

Fig. 10. Adsorption mechanism of Cu(II) and Cd(II) onto GO.

Table 6
Comparison of Cu(II) and Cd(II) adsorption on GO and other adsorbents

Name of adsorbent	pH	Metal ion	q_{max} (mg/g)	References
$MnFe_2O_3$@TiO_2-rGO	5.7	Cu^{2+}	118.45	[73]
GO	5.0	Cu^{2+}	46.6	[74]
GO-PAMAM	5.6	Cu^{2+}	38.4	[75]
GO aerogel	6.3	Cu^{2+}	19.7	[76]
CSGO	6.3	Cu^{2+}	53.7	[77]
ZnO nanoparticles	6.0	Cd^{2+}	71.5	[78]
Magnetic graphene oxide/MgAl-layered double hydroxide	5–6	Cu^{2+}	45.05	[79]
		Cd^{2+}	23.04	
rGO-PDTC/Fe_3O_4	5.0	Cu^{2+}	113.64	[80]
	6.0	Cd^{2+}	116.28	
GO	6.0	Cu^{2+}	193.05	This study
	7.0	Cd^{2+}	231.45	This study

kinetic model. The maximum Cu(II) and Cd(II) removal capacity were 193.05 and 231.45 mg/g, respectively. Change of Gibb's free energy, enthalpy and entropy were determined by van't Hoff equation and found that the adsorption processes were exothermic and spontaneous in nature. Exhausted adsorbent was regenerated by treatment with 2% HCl and reused satisfactorily. However, further studies are warranted for its development as a commercial adsorbent.

Acknowledgements

The authors would like to thank the Department of Applied Chemistry and Chemical Engineering, Institute of Leather Engineering and Technology (ILET), University of Dhaka and Atomic Energy Center, Bangladesh Atomic Energy Commission, Dhaka for providing laboratory facilities and testing supports.

References

[1] I.M. Kenawy, M.A.H. Hafez, M.A. Ismail, M.A. Hashem, Adsorption of Cu(II), Cd(II), Hg(II), Pb(II) and Zn(II) from aqueous single metal solutions by guanyl-modified cellulose, Int. J. Biol. Macromol., 107 (2018) 1538–1549.
[2] M.A. Hashem, M. Hasan, M.A. Momen, S. Payel, M.S. Nur-A-Tomal, Water hyacinth biochar for trivalent chromium adsorption from tannery wastewater, Environ. Sustainability Indic., 5 (2020) 100022, doi: 10.1016/j.indic.2020.100022.
[3] A.A. Alqadami, Mu. Naushad, M.A. Abdalla, T. Ahamad, Z.A. ALOthman, S.M. Alsehri, A.A. Ghfar, Efficient removal of toxic metal ions from wastewater using a recyclable nanocomposite: a study of adsorption parameters and interaction mechanism, J. Cleaner Prod., 156 (2017) 426–436.
[4] T. Benvenuti, M.A. Siqueira Rodrigues, A.M. Bernardes, J. Zoppas-Ferreira, Closing the loop in the electroplating industry by electrodialysis, J. Cleaner Prod., 155 (2017) 130–138.
[5] S.L. Cardoso, C.S.D. Costa, E. Nishikawa, M.G.C. da Silva, M.G.A. Vieira, Biosorption of toxic metals using the alginate extraction residue from the brown algae *Sargassum filipendula* as a natural ion-exchanger, J. Cleaner Prod., 165 (2017) 491–499.
[6] P.S. Kumar, S. Ramalingam, V. Sathyaselvabala, S.D. Kirupha, A. Murugesan, S. Sivanesan, Removal of cadmium(II) from aqueous solution by agricultural waste cashew nut shell, Korean J. Chem. Eng., 29 (2012) 756–768.
[7] A.B.P. Marín, M.I. Aguilar, J.F. Ortuño, V.F. Meseguer, J. Sáez, M. Lloréns, Biosorption of Zn(II) by orange waste in batch and packed-bed systems, J. Chem. Technol. Biotechnol., 85 (2010) 1310–1318.
[8] Z. Gokalp, D. Mohammed, Assessment of heavy metal pollution in Heshkaro stream of Duhok city, Iraq, J. Cleaner Prod., 237 (2019) 117681, doi: 10.1016/j.jclepro.2019.117681.
[9] E.A.A. Omodele, A.G. Adewale, M.M. Mikaila, A Mini-Review on the Application of Alumina Nanoparticles for Water Treatment, International Science Conference, Faculty of Science Auditorium, Federal University Oye-Ekiti, Ekiti State, Nigeria, 2019, pp. 4–8.
[10] K. Nithya, A. Sathish, P.S. Kumar, Packed bed column optimization and modeling studies for removal of chromium ions using chemically modified *Lantana camara* adsorbent, J. Water Process Eng., 33 (2019) 101069, doi: 10.1016/j.jwpe.2019.101069.
[11] K. Banerjee, A novel agricultural waste adsorbent, watermelon shell for the removal of copper from aqueous solutions, Iran. J. Energy Environ., 3 (2012) 143–156.
[12] P. Saha, S. Chowdhury, Insight Into Adsorption Thermodynamics, M. Tadashi, Ed., Thermodynamics, InTechOpen, 2011. Available at: http://www.intechopen.com/books/thermodynamics/insight-into-adsorption-thermodynamics
[13] V.M. Marín-Rangel, R. Cortés-Martínez, R.A. Cuevas Villanueva, M.G. Garnica-Romo, H.E. Martínez-Flores, As(V) biosorption in an aqueous solution using chemically treated lemon (*Citrus aurantifolia* Swingle) residues, J. Food Sci., 77 (2012) 10–14.
[14] V. Mishra, C. Balomajumder, V.K. Agarwal, Kinetics, Mechanistic and thermodynamics of Zn(II) ion sorption: a modeling approach, CLEAN - Soil Air Water, 40 (2012) 718–727.
[15] T.A.H. Nguyen, H.H. Ngo, W.S. Guo, J. Zhang, S. Liang, Q.Y. Yue, Q. Li, T.V. Nguyen, Applicability of agricultural waste and by-products for adsorptive removal of heavy metals from wastewater, Bioresour. Technol., 148 (2013) 574–585.
[16] C. Lei, X. Zhu, B. Zhu, C. Jiang, Y. Le, J. Yu, Superb adsorption capacity of hierarchical calcined Ni/Mg/Al layered double hydroxides for Congo red and Cr(VI) ions, J. Hazard. Mater., 321 (2017) 801–811.
[17] A. Mandal, N. Singh, Kinetic and isotherm error optimization studies for adsorption of atrazine and imidacloprid on bark

of *Eucalyptus tereticornis* L., J. Environ. Sci. Health., Part B, 51 (2016) 192–203.
[18] M. Ghaedi, A.G. Nasab, S. Khodadoust, M. Rajabi, S. Azizian, Application of activated carbon as adsorbents for efficient removal of methylene blue: kinetics and equilibrium study, J. Ind. Eng. Chem., 20 (2014) 2317–2324.
[19] L. Wu, W. Wan, Z. Shang, X. Gao, N. Kobayashi, G. Luo, Z. Li, Surface modification of phosphoric acid activated carbon by using non-thermal plasma for enhancement of Cu(II) adsorption from aqueous solutions, Sep. Purif. Technol., 197 (2018) 156–169.
[20] R.A. Figueroa, A. Leonard, A.A. Mackay, Modeling tetracycline antibiotic sorption to clays, Environ. Sci. Technol., 38 (2004) 476–483.
[21] L. Ai, Y. Zhou, J. Jiang, Removal of methylene blue from aqueous solution by montmorillonite/$CoFe_2O_4$ composite with magnetic separation performance, Desalination, 266 (2011) 72–77.
[22] J. Maity, S.K. Ray, Chitosan based nano composite adsorbent-synthesis, characterization and application for adsorption of binary mixtures of Pb(II) and Cd(II) from water, Carbohydr. Polym., 182 (2018) 159–171.
[23] R. Karthik, S. Meenakshi, Removal of Cr(VI) ions by adsorption onto sodium alginate-polyaniline nanofibers, Int. J. Biol. Macromol., 72 (2015) 711–717.
[24] Jumina, Y. Priastomo, H.R. Setiawan, Mutmainah, Y.S. Kurniawan, K. Ohto, Simultaneous removal of lead(II), chromium(III), and copper(II) heavy metal ions through an adsorption process using C-phenylcalix[4]pyrogallolarene material, J. Environ. Chem. Eng., 8 (2020) 103971, doi: 10.1016/j.jece.2020.103971.
[25] S. Raghav, D. Kumar, Adsorption equilibrium, kinetics, and thermodynamic studies of fluoride adsorbed by tetrametallic oxide adsorbent, J. Chem. Eng. Data, 63 (2018) 1682–1697.
[26] S. Ghosh, D. Mitra, Elimination of Chromium(VI) from Waste Water Using Various Biosorbents, A. Sarma, V. Singh, R. Bhattacharjya, S. Kartha, Eds., Urban Ecology, Water Quality and Climate Change, Water Science and Technology Library, Vol 84, Springer, Cham, 2018. Available at: https://doi.org/10.1007/978-3-319-74494-0_20
[27] S. Mitra, A. Sarkar, S. Sen, Removal of chromium from industrial effluents using nanotechnology: a review, Nanotechnol. Environ. Eng., 2 (2017) 11, doi: 10.1007/s41204-017-0022-y.
[28] H. Hadi Najafabadi, M. Irani, L. Roshanfekr Rad, A. Heydari Haratameh, I. Haririan, Removal of Cu^{2+}, Pb^{2+} and Cr^{6+} from aqueous solutions using a chitosan/graphene oxide composite nanofibrous adsorbent, RSC Adv., 5 (2015) 16532–16539.
[29] H. Wei, J. Zhu, S. Wu, S. Wei, Z. Guo, Electrochromic polyaniline/graphite oxide nanocomposites with endured electrochemical energy storage, Polymer (Guildf)., 54 (2013) 1820–1831.
[30] F. Guo, Y. Liu, H. Wang, G. Zeng, X. Hu, B. Zheng, T. Li, X. Tan, S. Wang, M. Zhang, Adsorption behavior of Cr(VI) from aqueous solution onto magnetic graphene oxide functionalized with 1,2-diaminocyclohexanetetraacetic acid, RSC Adv., 5 (2015) 45384–45392.
[31] X. Liu, Y. Zhou, W. Nie, L. Song, P. Chen, Fabrication of hydrogel of hydroxypropyl cellulose (HPC) composited with graphene oxide and its application for methylene blue removal, J. Mater. Sci., 50 (2015) 6113–6123.
[32] A.R. Kamali, D.J. Fray, Molten salt corrosion of graphite as a possible way to make carbon nanostructures, Carbon N. Y., 56 (2013) 121–131.
[33] K.R. Parmar, I. Patel, S. Basha, Z.V.P. Murthy, Synthesis of acetone reduced graphene oxide/Fe_3O_4 composite through simple and efficient chemical reduction of exfoliated graphene oxide for removal of dye from aqueous solution, J. Mater. Sci., 49 (2014) 6772–6783.
[34] L. Huang, Y. Wang, J. Tang, Y. Wang, J. Liu, Z. Huang, J. Jiao, W. Wang, J.K. Matt, B.A. Laurence, A new graphene nanocomposite to improve the electrochemical properties of magnesium-based amorphous alloy, Mater. Lett., 160 (2015) 104–108.
[35] R. Wijaya, G. Andersan, S. Permatasari Santoso, W. Irawaty, Green reduction of graphene oxide using kaffir lime peel extract (*Citrus hystrix*) and its application as adsorbent for methylene blue, Sci. Rep., 10 (2020) 1–9, doi: 10.1038/s41598-020-57433-9.
[36] X. Yang, T. Zhou, B. Ren, A. Hursthouse, Y. Zhang, Removal of Mn(II) by sodium alginate/graphene oxide composite double-network hydrogel beads from aqueous solutions, Sci. Rep., 8 (2018) 1–16.
[37] X. Liu, R. Ma, X. Wang, Y. Ma, Y. Yang, L. Zhuang, S. Zhang, R. Jehan, J. Chen, X. Wang, Graphene oxide-based materials for efficient removal of heavy metal ions from aqueous solution: a review, Environ. Pollut., 252 (2019) 62–73.
[38] A. Abu-Nada, G. McKay, A. Abdala, Recent advances in applications of hybrid graphene materials for metals removal from wastewater, Nanomaterials, 10 (2020) 595, doi: 10.3390/nano10030595.
[39] C.S. Nkutha, P.N. Diagboya, F.M. Mtunzi, E.D. Dikio, Application of eco-friendly multifunctional porous graphene oxide for adsorptive sequestration of chromium in aqueous solution, Water Environ. Res., 92 (2020) 1070–1079.
[40] S. Ahmed, Fatema-Tuj-Zohra, M.M. Mahdi, D.M. Mahmudunnabi, T.R. Choudhury, M.Z. Alam, M. Nurnabi, Synthesis and characterization of graphene oxide for removal of Cr(III) from tannery effluent, Desal. Water Treat., 244 (2021) 201–211.
[41] B.I. Olu-owolabi, P.N. Diagboya, W.C. Ebaddan, Mechanism of Pb^{2+} removal from aqueous solution using a nonliving moss biomass, Chem. Eng. J., 195–196 (2012) 270–275.
[42] H. Zhu, T. Chen, J. Liu, D. Li, Adsorption of tetracycline antibiotics from an aqueous solution onto graphene oxide/calcium alginate composite fibers, RSC Adv., 8 (2018) 2616–2621.
[43] Y. Fei, Y. Li, S. Han, J. Ma, Adsorptive removal of ciprofloxacin by sodium alginate/graphene oxide composite beads from aqueous solution, J. Colloid Interface Sci., 484 (2016) 196–204.
[44] N.I. Zaaba, K.L. Foo, U. Hashim, S.J. Tan, W.W. Liu, C.H. Voon, Synthesis of graphene oxide using modified Hummers method: solvent influence, Procedia Eng., 184 (2017) 469–477.
[45] M.Z. Iqbal, A.A. Abdala, Thermally reduced graphene: Synthesis, characterization and dye removal applications, RSC Adv., 3 (2013) 24455–24464.
[46] J. Wang, B. Chen, Adsorption and coadsorption of organic pollutants and a heavy metal by graphene oxide and reduced graphene materials, Chem. Eng. J., 281 (2015) 379–388.
[47] C. Valencia, C.H. Valencia, F. Zuluaga, M.E. Valencia, J.H. Mina, C.D. Grande-Tovar, Synthesis and application of scaffolds of chitosan-graphene oxide by the freeze-drying method for tissue regeneration, Molecules, 23 (2018) 2651, doi: 10.3390/molecules23102651.
[48] D.M. Mahmudunnabi, M.Z. Alam, M. Nurnabi, Removal of TURQUOISE GN from aqueous solution using graphene oxide, Desal. Water Treat., 174 (2020) 389–399.
[49] R. Jabari, M. Jahanshahi, A. Rashidi, A. Asghar, Applied surface science synthesize and characterization of graphene nanosheets with high surface area and nano-porous structure, Appl. Surf. Sci., 276 (2013) 672–681.
[50] S. Zhang, H. Wang, J. Liu, C. Bao, Measuring the specific surface area of monolayer graphene oxide in water, Mater. Lett., 261 (2019) 127098, doi: 10.1016/j.matlet.2019.127098.
[51] I. Sengupta, S. Chakraborty, M. Talukdar, S.K. Pal, S. Chakraborty, Thermal reduction of graphene oxide: how temperature influences purity, J. Mater. Res., 33 (2018), doi: 10.1557/jmr.2018.338.
[52] S. Lv, Q. Zhou, Y. Li, Y. He, H. Zhao, Tanning performance and environmental effects of nanosized graphene oxide tanning agent, Clean Technol. Environ. Policy, 18 (2016) 1997–2006.
[53] R.P. Mohubedu, P.N.E. Diagboya, C.Y. Abasi, E.D. Dikio, F. Mtunzi, Magnetic valorization of biomass and biochar of a typical plant nuisance for toxic metals contaminated water treatment, J. Cleaner Prod., 209 (2018) 1016–1024.
[54] P.N. Diagboya, E.D. Dikio, Dynamics of mercury solid phase extraction using *Barbula lambarenensis*, Environ. Technol. Innovation, 9 (2018) 275–284.

[55] P.R. Sera, P.N. Diagboya, S.O. Akpotu, F.M. Mtunzi, T.B. Chokwe, Potential of valourized *Moringa oleifera* seed waste modified with activated carbon for toxic metals decontamination in conventional water treatment, Bioresour. Technol. Rep., 16 (2021) 100881, doi: 10.1016/j.biteb.2021.100881.
[56] P.N. Diagboya, E.D. Dikio, Scavenging of aqueous toxic organic and inorganic cations using novel facile magneto-carbon black-clay composite adsorbent, J. Cleaner Prod., 180 (2018) 71–80.
[57] P. Tan, J. Sun, Y. Hu, Z. Fang, Q. Bi, Y. Chen, J. Cheng, Adsorption of Cu^{2+}, Cd^{2+} and Ni^{2+} from aqueous single metal solutions on graphene oxide membranes, J. Hazard. Mater., 297 (2015) 251–260.
[58] R.L. White, C.M. White, H. Turgut, A. Massoud, Z.R. Tian, Comparative studies on copper adsorption by graphene oxide and functionalized graphene oxide nanoparticles, J. Taiwan Inst. Chem. Eng., 85 (2018) 18–28.
[59] A. Jean Jacques, T. Eko Kevin, T. Guy Merlain, K. Daouda, K. Joseph Mbadcam, Adsorption study of Cu^{2+} ions from aqueous solution using kaolinite and metakaolinite, Int. J. Mod. Res. Eng. Technol., 3 (2018) 13–23.
[60] H. Patel, Fixed-bed column adsorption study: a comprehensive review, Appl. Water Sci., 9 (2019) 45, doi: 10.1007/s13201-019-0927-7.
[61] I.-H.T. Kuete, D.R.T. Tchuifon, G.N. Ndifor-Angwafor, A.T. Kamdem, S.G. Anagho, Kinetic, isotherm and thermodynamic studies of the adsorption of thymol blue onto powdered activated carbons from garcinia cola nut shells impregnated with H_3PO_4 and KOH: non-linear regression analysis, J. Encapsulation Adsorpt. Sci., 10 (2020) 1–27.
[62] M.K. Rai, B.S. Giri, Y. Nath, H. Bajaj, S. Soni, R.S. Singh, B.N. Rai, Adsorption of hexavalent chromium from aqueous solution by activated carbon prepared from almond shell: Kinetics, equilibrium and thermodynamics study, J. Water Supply Res. Technol. AQUA, 67 (2018) 724–737.
[63] N.K. Mondal, S. Chakraborty, Adsorption of Cr(VI) from aqueous solution on graphene oxide (GO) prepared from graphite: equilibrium, kinetic and thermodynamic studies, Appl. Water Sci., 10 (2020) 1–10, doi: 10.1007/s13201-020-1142-2.
[64] W.J. Weber, P.M. McGinley, E.K. Lynn, A distributed reactivity model for sorption by soils and Sediments. 1. Conceptual basis and equilibrium assessments, Environ. Sci. Technol., 10 (1992) 1955–1962.
[65] T.A. Saleh, Isotherm, kinetic, and thermodynamic studies on Hg(II) adsorption from aqueous solution by silica- multiwall carbon nanotubes, Environ. Sci. Pollut. Res., 22 (2015) 16721–16731.
[66] E. Aranda-García, G.M. Chávez-Camarillo, E. Cristiani-Urbina, Effect of ionic strength and coexisting ions on the biosorption of divalent nickel by the acorn shell of the oak *Quercus crassipes* humb. & bonpl., Processes, 8 (2020) 1229 (1–17), doi: 10.3390/pr8101229.
[67] Z.P. Zanele, F.M. Mtunzi, S.M. Nelana, A.N. Ebelegi, N. Ayawei, E.D. Dikio, D. Wankasi, P.N. Diagboya, Metals and antibiotics as aqueous sequestration targets for magnetic polyamidoamine-grafted SBA-15, Langmuir, 37 (2021) 9764–9773.
[68] S. Kebede, Groundwater in Ethiopia: Features, Numbers and Opportunities, Springer, Berlin, Heidelberg, 2013, pp. 1–285. doi: 10.1007/978-3-642-30391-3.
[69] A. Siddique, A.K. Nayak, J. Singh, Synthesis of $FeCl_3$-activated carbon derived from waste *Citrus limetta* peels for removal of fluoride: an eco-friendly approach for the treatment of groundwater and bio-waste collectively, Groundwater Sustainable Dev., 10 (2020) 100339, doi: 10.1016/j.gsd.2020.100339.
[70] M.E. Ali, M.E. Hoque, S.K. Safdar Hossain, M.C. Biswas, Nanoadsorbents for wastewater treatment: next generation biotechnological solution, Int. J. Environ. Sci. Technol., 17 (2020) 4095–4132.
[71] L. Li, C. Luo, X. Li, H. Duan, X. Wang, Preparation of magnetic ionic liquid/chitosan/graphene oxide composite and application for water treatment, Int. J. Biol. Macromol., 66 (2014) 172–178.
[72] F. Shoushtarian, M.R.A. Moghaddam, E. Kowsari, Efficient regeneration/reuse of graphene oxide as a nanoadsorbent for removing Basic red 46 from aqueous solutions, J. Mol. Liq., 312 (2020) 113386, doi: 10.1016/j.molliq.2020.113386.
[73] L. Chang, Y. Pu, P. Jing, Y. Cui, G. Zhang, S. Xu, B. Cao, J. Guo, F. Chen, C. Qiao, Magnetic core-shell $MnFe_2O_4$@TiO_2 nanoparticles decorated on reduced graphene oxide as a novel adsorbent for the removal of ciprofloxacin and Cu(II) from water, Appl. Surf. Sci., 541 (2021) 148400, doi: 10.1016/j.apsusc.2020.148400.
[74] S.T. Yang, Y. Chang, H. Wang, G. Liu, S. Chen, Y. Wang, Y. Liu, A. Cao, Folding/aggregation of graphene oxide and its application in Cu^{2+} removal, J. Colloid Interface Sci., 351 (2010) 122–127.
[75] Y. Yuan, G. Zhang, Y. Li, G. Zhang, F. Zhang, X. Fan, Poly(amidoamine) modified graphene oxide as an efficient adsorbent for heavy metal ions, Polym. Chem., 4 (2013) 2164–2167.
[76] X. Mi, G. Huang, W. Xie, W. Wang, Y. Liu, J. Gao, Preparation of graphene oxide aerogel and its adsorption for Cu^{2+} ions, Carbon N. Y., 50 (2012) 4856–4864.
[77] Y. Wang, X. Liu, H. Wang, G. Xia, W. Huang, R. Song, Microporous spongy chitosan monoliths doped with graphene oxide as highly effective adsorbent for methyl orange and copper nitrate ($Cu(NO_3)_2$) ions, J. Colloid Interface Sci., 416(2014) 243–251.
[78] N. Kataria, V.K. Garg, Optimization of Pb(II) and Cd(II) adsorption onto ZnO nanoflowers using central composite design: isotherms and kinetics modelling, J. Mol. Liq., 271 (2018), doi: 10.1016/j.molliq.2018.08.135.
[79] Q. Huang, Y. Chen, H. Yu, L. Yan, J. Zhang, B. Wang, B. Du, L. Xing, Magnetic graphene oxide/MgAl-layered double hydroxide nanocomposite: one-pot solvothermal synthesis, adsorption performance and mechanisms for Pb^{2+}, Cd^{2+}, and Cu^{2+}, Chem. Eng. J., 341 (2018) 1–9.
[80] W. Fu, Z. Huang, Magnetic dithiocarbamate functionalized reduced graphene oxide for the removal of Cu(II), Cd(II), Pb(II), and Hg(II) ions from aqueous solution: synthesis, adsorption, and regeneration, Chemosphere, 209 (2018) 449–456.

Supporting information

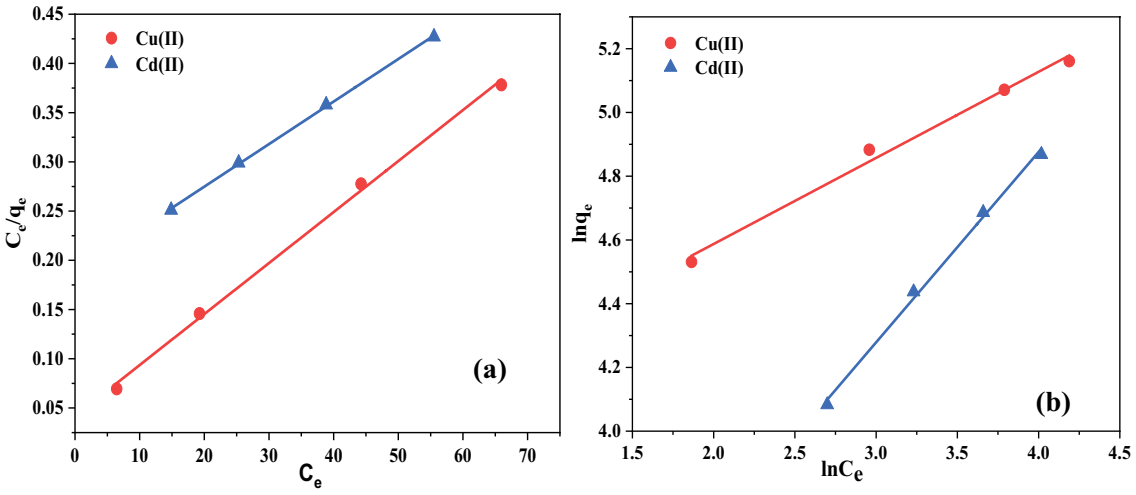

Fig. S1. (a) Langmuir and (b) Freundlich isotherm models for Cu(II) and Cd(II) adsorption on GO.

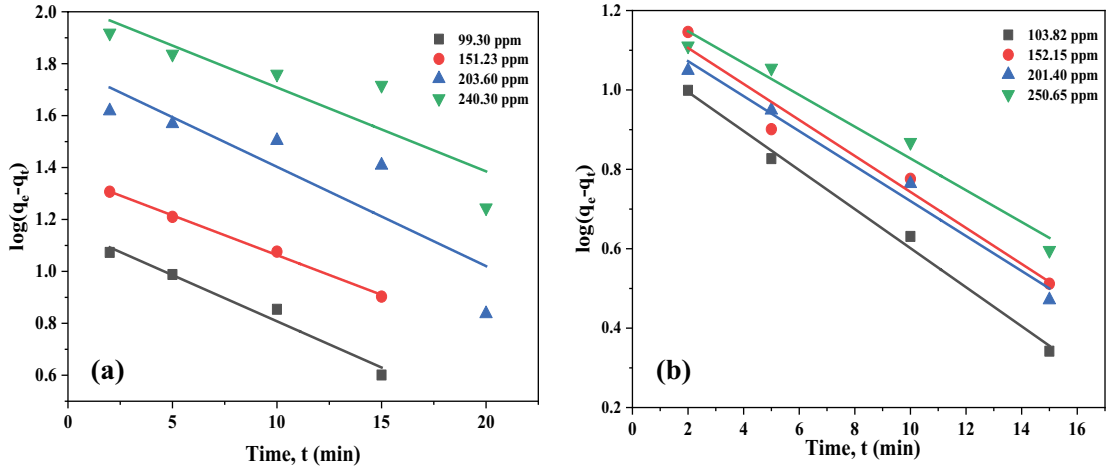

Fig. S2. Kinetic models of pseudo-first-order (a) Cu(II) and (b) Cd(II) reaction for adsorption on GO.

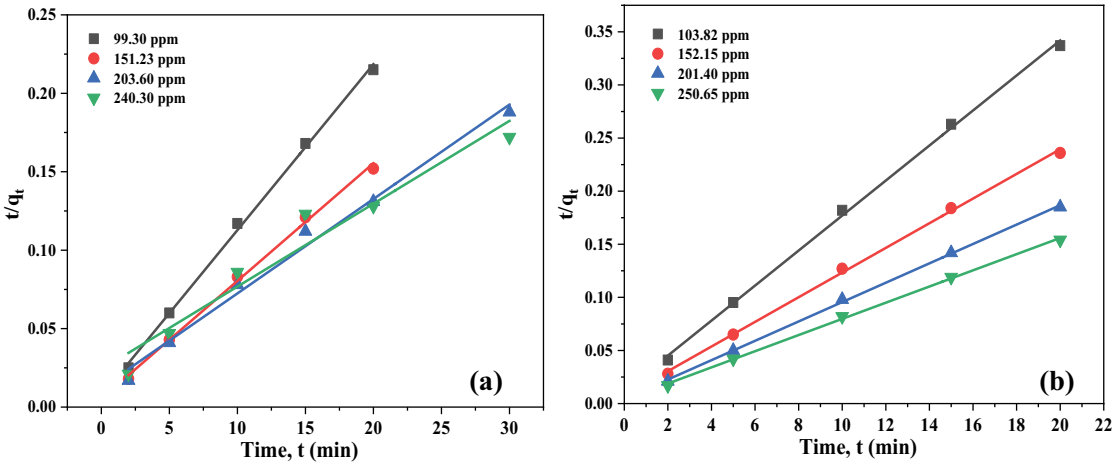

Fig. S3. Kinetic models of pseudo-second-order (a) Cu(II) and (b) Cd(II) reaction for adsorption on GO.